# Flight Optimization Algorithms for Aerial LiDAR Capture for Urban Infrastructure Model Generation

Tommy Hinks[1]; Hamish Carr[2]; and Debra F. Laefer, M.ASCE[3]

**Abstract:** Aerial light detection and ranging (LiDAR) offers the potential to autogenerate detailed, three-dimensional (3D) models of the built environment in urban settings. Autogeneration is needed as manual generation is not economically feasible for large areas, and such models are needed for a wide range of applications from improved noise and pollution prediction to disaster mitigation modeling and visualization. Current laser scanning hardware and the dense geometry of urban environments are two major constraints in LiDAR scanning. This paper outlines the difficulties related to effective surface data capture, with emphasis on vertical surfaces, in an urban environment for the purpose of 3D modeling. A flight planning strategy to overcome these difficulties is presented, along with a case study of a data set collected with this strategy. The main conclusions of this study are that an appropriate amount of strip overlap, together with a flight path diagonal to the underlying street grid produces a vastly enhanced level of detail on vertical surfaces, beyond what has been previously available.

**DOI:** 10.1061/(ASCE)0887-3801(2009)23:6(330)

**CE Database subject headings:** Aerial surveys; Remote sensing; Three-dimensional models; Geographic information systems; Urban areas; Infrastructure.

## Introduction

Aerial laser scanning is a relatively new technique for spatial data acquisition. Aerial laser scanner systems are based on the principles of light detection and ranging (LiDAR). The return times of laser pulses emitted from an aircraft platform toward the ground are measured, and the corresponding ranges are computed. Knowledge of the aircraft position [from global positioning system (GPS)] and rotation (from inertial navigation system) enable the conversion of ranges to point positions. The product of aerial laser scanning is a dense cloud of three-dimensional (3D) points, commonly referred to as a *point cloud*. The points are samples from the surfaces beneath the aircraft (e.g., bare earth, buildings, vegetation, and other objects). The denseness of laser scanner data offers the opportunity for a faithful reconstruction of the surfaces; for further details see Baltsavias (1999a) and Wehr and Lohr (1999). LiDAR technology has been used in many areas of applications such as (1) geographic information system (GIS) content generation; (2) disaster response and damage assessment (Laefer and Pradhan 2006); (3) flood plain mapping (Hollaus et al. 2005); (4) forestry (Andersen et al. 2005); (5) urban modeling (Forlani et al. 2006)l; and (6) building condition assessment (Laefer et al. 2009).

Urban Planners and Civil Engineers require large-scale 3D geometric models of urban areas for a wide range of applications, including such seemingly disparate subjects as predictive noise and pollution models and disaster mitigation. As an example, in the event of sudden infrastructure changes, such applications require accurate geometric models, and in a postdisaster scenario, the models must be acquired rapidly as well. Increasingly, large-scale computing efforts are being applied to urban planning and disaster management. These range from optimizing single-incident fire department responses to predicting and mitigating regional flooding effects (Kevany 2003; Hollaus et al. 2005). Many of these efforts have relied upon GIS with substantial manual input. Typically, governmental agencies maintain base maps of their jurisdiction. The majority of these base maps are limited to two-dimensional (2D) representations, with 3D functionalities being limited to a highly narrow set of applications. In coming decades, as population and urbanization expand, threats to quality of life issues (e.g., preservation of natural resources, green spaces, air quality) will continue to intensify. As such, better computer modeling capabilities related to these topics will be needed. Aerial LiDAR technology holds the potential for rapid autogeneration of 3D models.

Because aerial LiDAR requires expensive hardware, the actual scanning is often conducted by specialized surveyors, who are contracted to scan specific areas of interest. As the scanning aircraft moves along its path, it scans a strip on the ground. The strip width depends on aircraft altitude and scanner specifications. Most often, the area of interest is wider than a single strip, requiring several passes to be flown over the area of interest, to ensure that the entirety of the area is covered by at least one strip. The path taken by the aircraft during the scan is referred to as the *flight plan*. The flight plan also includes such parameters as aircraft altitude and speed, which in turn have a large impact on the resulting data quality. While there are potentially many different

[1]Doctoral Candidate, School of Computer Science and Informatics, Univ. College Dublin, Belfield, Dublin 4, Ireland.

[2]Tenured Lecturer, School of Computer Science and Informatics, Univ. College Dublin, Belfield, Dublin 4, Ireland.

[3]Tenured Lecturer and Lead Principal Investigator, Urban Modelling Group, School of Architecture, Landscape, and Civil Engineering, Univ. College Dublin, Newstead, Room G25, Belfield, Dublin 4, Ireland (corresponding author). E-mail: debra.laefer@ucd.ie

Note. This manuscript was submitted on June 18, 2007; approved on June 15, 2009; published online on October 15, 2009. Discussion period open until April 1, 2010; separate discussions must be submitted for individual papers. This paper is part of the ***Journal of Computing in Civil Engineering***, Vol. 23, No. 6, November 1, 2009. ©ASCE, ISSN 0887-3801/2009/6-330–339/$25.00.

flight plans that ensure complete coverage, focus tends to be on achieving coverage with minimal ground data redundancy between the strips. Generally, some minimal strip overlap is recommended to compensate for navigational errors and the roll and pitch of the aircraft. Anything beyond that strip overlap has been considered redundant and unnecessary. This paper will present a rethinking of this position and show mathematically and through a case study how a fundamentally improved data set can be collected, one that opens new vistas for 3D urban modeling, which is highly dependent on accurate vertical capture.

## Background

LiDAR is an active remote sensing technology used to collect topographic data. The data are collected with aircraft-mounted lasers capable of recording distance measurements at a rate of many thousand pulses per second. Instruments collect range data from known locations as the aircraft moves along the flight path. A high-precision GPS antenna, mounted on the aircraft, is used to determine the spatial positions of the aircraft, and so indirectly the positions of the data points collected, since these are offset from the aircraft at given directions and distances. Data can easily be converted into an elevation map by finding the maximum elevation for each patch in the ground plane (Baltsavias 1999b). The end product is accurate and geographically registered with respect to longitude, latitude, and elevation from the mean sea level, and typically presented in a Cartesian coordinate system with $(x,y,z)$-coordinates for every data point.

Airborne LiDAR is capable of providing both horizontal and vertical information at high spatial resolutions and vertical accuracies. In the horizontal plane, airborne LiDAR data are accurate to $+/-15$ cm for range measurements and $+/-1.5$ m (worst case scenario) in the ground plane, although systems are sometimes marketed as having higher accuracy than this (e.g., Latypov 2002). The extent of LiDAR point density is dependent on aircraft height and system related factors, such as platform velocity, sampling frequency (scan rate), and field of view (Axelsson 1999). The point density needs to be adjusted according to the application so that sufficient information is harvested, while not collecting excessively detailed data.

One of the benefits of aerial LiDAR is that it is possible to collect 3D information for thousands of buildings in only a few hours. The data can then be tied directly to a GIS base map. Such an approach, however, is restricted currently to a 2D consideration of the community. Subsequent building models derived from the data are typically of an extruded or instantiated nature and do not reflect the true geometric and material characteristics of the façades and other vertical faces. Vertical building features are known to be essential in the modeling of a variety of topics including blast-energy dissipation, urban wind tunnels, and pollution modeling (Maas and Vosselman 1999; Rottensteiner 2003). A current alternative is modeling urban geometry by hand, using modeling software, but this is both slow and often inaccurate (Hamill and O'Sullivan 2003).

As laser beams travel away from the scanner toward objects in the scene, the beam widens. This widening, often referred to as *beam divergence*, effectively means that range sampling is not done at a single point, but rather over a small area, referred to as the *laser footprint*. If the laser footprint is large, the range measurement is not representative of a single point, but rather of a larger patch, introducing averaging errors, when the sample is treated as a single point. The laser footprint can be approximated by the expression $A_L=h\gamma$, where $A_L$ is the laser footprint in meters, $h$ is the altitude of the scanner in meters, and $\gamma$ is the beam divergence in radians (Baltsavias 1999b). Modern LiDAR systems have beam divergence angles of about 0.5 milliradians (Liu et al. 2005). The relatively low heights used in urban scans, combined with the small beam divergence angles of modern hardware, result in laser footprint areas that are close to singular points. For a scanner at a height of 300 m with the above quoted beam divergence, the laser footprint is 15 cm, which is considered small in relation to the objects of interest (i.e., the buildings). Hence, the beam divergence error is negligible and, therefore, ignored in the following discussion.

Traditionally, aerial LiDAR scans have provided high quality data only on horizontal surfaces. Vertical surfaces are harder to capture accurately, principally because the laser beam strikes them obliquely, but also because of shadowing effects. Früh and Zakhor (2003) merged terrestrial laser scans of vertical surfaces with aerial data in an attempt to overcome the problems associated with obliquity in aerial LiDAR. This approach, however, is not always feasible. The ground-data acquisition is much slower than flying over an area since it requires traveling along the streets at ground level. Also, in the case of sudden infrastructure changes (e.g., earthquake or blast explosion), acquiring the ground scans may be impossible.

For aerial LiDAR scans both obliquity and shadows generate *dead zones*—regions in which data capture are either poor or nonexistent. In particular, dead zones are generated by scan obliquity, façade shadows (building self-shadows), and canyon shadows (interbuilding shadows). Thus, collecting densely sampled data for vertical surfaces involves planning a flight path to minimize these effects. The main body of this paper, therefore, presents an analysis of these geometric constraints and provides recommendations on how to plan a suitable flight path to minimize these negative effects for a particular urban environment.

### Aerial LiDAR Data Processing

Visualization is crucial to understanding and analyzing large data sets, and is therefore, a critical issue in large-scale urban planning. Visualizing the large data sets involved in city-scale surveys is challenging. On a city scale, point clouds may contain hundreds of millions of points. These point clouds are unsuitable for immediate visualization and engineering purposes because of their unstructured nature. The task of visualizing LiDAR data can be divided into two areas: (1) reconstructing surfaces (e.g., Kazhdan et al. 2006) from point clouds—a noise-sensitive procedure, the success of which is largely dependent on the quality of the sampled points and (2) visualization of reconstructed surfaces, where efficient scene representations and caching methods must be employed in order to allow modern rendering engines to cope with the enormous data sets involved.

Before surface reconstruction can take place and a topological structure can be deduced, filtering of raw point data are necessary. Current practice involves performing an initial culling or *segmentation* of point samples and keeping only the ones that are (believed to be) on objects of interest. For urban scans, most often only man-made structures are of interest, and of these buildings are typically the main objects of study. However, LiDAR instruments capture point samples on all objects within their line-of-sight, including vegetation, vehicles, and street furniture. Therefore, building segmentation has received considerable atten-

tion over the last decade as LiDAR has emerged a serious alternative for city-scale modeling (e.g., Haala and Brenner 1999; Filin et al. 2007).

For a long time, such segmentation methods (e.g., Vosselman et al. 2004) did not rely on point samples being taken on vertical surfaces (i.e., building walls). Building walls were mainly detected by identifying height differences on a resampled 2D grid. These approaches have several drawbacks. First of all, they fail to correctly position walls in the presence of overhanging roofs, since the height difference is detected at the most overhanging edge of the roof, whereas the wall might be positioned several meters inside this edge. Second, such methods find it difficult to distinguish building walls, when these are close to other tall objects, such as trees. More recent segmentation methods exploit the fact that modern aerial LiDAR data captures points on building walls (Dorninger and Nothegger 2007). These authors suggest that lower aircraft altitude and greater strip overlap generates better data quality on vertical surfaces, but do not develop the idea in detail or discuss how to plan flights so as to maximize vertical surface scan quality.

Baltsavias (1999b) and others note that the spacing between captured point samples is not uniform. Typically the sampling is regarded as random, and sometimes the irregularity is dealt with by interpolating values to a regular grid (Forlani et al. 2006). However, nowhere is sampling density mentioned in relation to flight planning, where it can be used to obtain a more uniform sampling quality and strike a balance between flight strip overlap and data quality, as well as provide previously missing building wall data. The sampling analysis presented in this paper shows how sampling patterns behave and how this can be used to design more optimal flight plans for urban scans.

## Analyzing Sampling Resolution

Resolution is a measurement of sampling quality. In the spatial context, resolution can be measured as the number of sampled data points in a given area or a given unit of length, or reciprocally as the area or unit length per point. Since scanning resolution may not be uniform, with respect to width (across the flight track) and length (along the flight track), a discussion of resolution as a linear measure, with respect to these two directions, is presented herein.

Contractors carrying out aerial LiDAR scans typically quote the quality of the data obtained as scan points per square meter. For purposes herein outlined, this must first be converted to *linear resolution* ($R_L$), the resolution in the along-track direction, which is assumed to be constant and depends on the velocity of the aircraft and the laser scan rate. Second, conversion into *horizontal resolution* ($R_H$), the sample spacing at ground level in the across-track direction is necessary. Finally conversion into *vertical resolution*, the vertical sample spacing on building sides must occur. Of these, the first two will be discussed next. The vertical resolution will be discussed in the section Vertical Scan Obliquity.

### Linear Resolution

The figure quoted for scan quality by contractors is notionally the number of scan points per square meter at *nadir* ($R_N$)—the point at ground level directly beneath the scanner. For the sake of argument it is assumed that $R_L=R_N$. This assumption is based on the fact that it is generally desirable to have uniform resolution throughout the entire set of collected scan points. As will be shown further on, this is impossible to achieve in practice because of variations in horizontal and vertical resolution in the across-track direction.

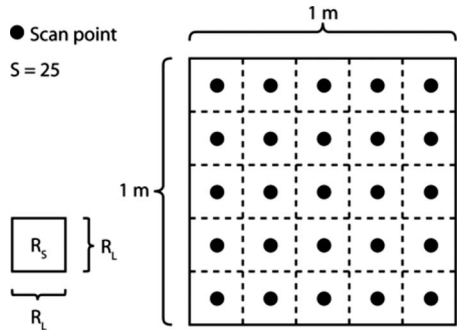


**Fig. 1.** Linear resolution and scan density

If $S$ is the number of scan points in 1 $m^2$, it follows that the relationship between $S$ and $R_L$ is $R_L=\sqrt{1/S}$, as shown in Fig. 1. Consequently the *surface resolution* ($R_S$) as a measure of the area that each scan point represents in the sampled scene is related to $R_L$, through the expression $R_S=R_L^2$. Features smaller than $R_S$ will not be recognizable in the data obtained. For example, if $R_S$ is in the order of meters squared per scan point, objects such as fire hydrants and waste bins will not be recognizable.

The ability to estimate the preflight linear resolution in the across-track direction is crucial to the conclusions presented in this paper. Unlike the along-track resolution, which is constant and is determined by the way the platform moves during the scanning process, the samples taken across-track are at uniformly spaced *angles*, not necessarily uniformly distributed distances. The following section derives an approximation for horizontal resolution based on flight-path altitude and angular resolution.

### Notional Horizontal Resolution

As the LiDAR scanner is flown above a city, laser pulses are emitted at small angular intervals up to 75° away from the vertical for current state-of-the-art scanners. Angular resolution is constant as the scanner sweeps along the across-track line (i.e., the difference in angle to the scanner from two consecutive scan points is constant). However, horizontal resolution at ground level is not constant. The distances between consecutive samples on the across-track line increase as the distance from nadir increases. Moving in the across-track direction away from nadir corresponds to increasing the offset angle $\theta_H$ from the vertical axis directly beneath the scanner. The distance $R_H$ between two consecutive samples depends on the altitude of the scanner ($h$), the offset angle from the vertical axis ($\theta_H$), and the angular resolution of the scanner ($\theta_L$). Fig. 2 illustrates the relationships between the parameters mentioned above. Note that the angle $\theta_L$ is not shown to scale in the illustrations to improve clarity. The horizontal resolution at nadir ($R_N$) is trivial to compute $R_N=h \tan \theta_L$.

The sine law is applied to triangle PRS (Fig. 2). Note that the right triangle PQS allows the substitution $\sin \alpha=\cos(90-\alpha)=\cos(\theta_H+\theta_L)$

$$\frac{\sin \alpha}{d}=\frac{\sin \theta_L}{R_H} \quad \text{or} \quad R_H \sin \alpha = d \sin \theta_L \tag{1}$$

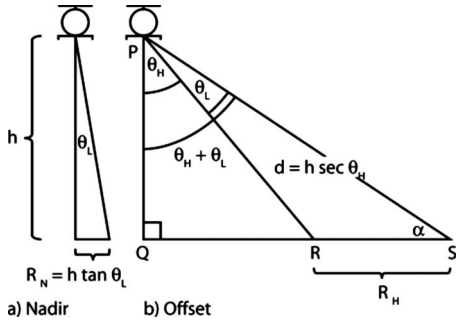


**Fig. 2.** Horizontal resolution

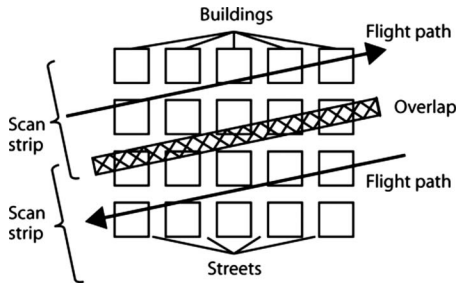


**Fig. 3.** Ideal urban grid pattern with standard flight pattern superimposed

$$R_H \cos(\theta_H + \theta_L) = h \sec \theta_H \sin \theta_L \tag{2}$$

$$R_H = \frac{h \sec \theta_H \sin \theta_L}{\cos(\theta_H + \theta_L)} = \frac{h \sec \theta_H \sin \theta_L}{\cos \theta_H \cos \theta_L - \sin \theta_H \sin \theta_L} \tag{3}$$

For small $\theta_L$ the denominator of the right-hand side of Eq. (3) is approximately equal to cos $\theta_H$. Using this approximation Eq. (3) can be rewritten as Eq. (4)

$$R_H = h \sin \theta_L \sec^2 \theta_H \tag{4}$$

Since $\theta_L$ is small sin $\theta_L$ is approximately equal to tan $\theta_L$ resulting in Eq. (5)

$$R_H = h \tan \theta_L \sec^2 \theta_H \quad \text{or} \quad R_H = R_N \sec^2 \theta_H \tag{5}$$

From this, the term $\sec^2 \theta_H$ can be interpreted as a scaling factor applied to the scan point spacing directly beneath the scanner. Let $\theta_W$ be the maximum offset angle for a given scanner; hence the largest occurring offset angle is $\theta_H = \theta_W$. For a given height, angular resolution, and scan width, the *effective* horizontal resolution (i.e., the worst case resolution, which occurs when $\theta_H = \theta_W$) can be computed. The expression for effective horizontal linear resolution ($R_W$) is obtained by inserting the height, angular resolution, and maximum offset into Eq. (5)

$$R_W = R_N \sec^2(\theta_W) \tag{6}$$

The LiDAR hardware used in the case study presented below is capable of angular resolutions in the order of 0.01° and maximum offset angles of 30° on each side. Inserting $\theta_W = 30°$ into Eq. (6) gives that the effective horizontal resolution is approximately 33% larger than horizontal resolution at nadir ($R_N$). Note that the scaling factor $\sec^2(\theta_W)$ does not depend on the angular resolution.

## Geometric Constraints on Flight Paths

There are five principal constraints on designing a suitable flight plan—urban geometry, flight geometry, vertical scan obliquity, self shadows, and street shadows. Each of these topics is treated in a separate subsection below, followed by a description of the ideal flight plan resulting from these constraints.

### *Urban Geometry*

Since the constraints on flight planning are principally geometric, characteristic geometry of urban environments must be acknowledged. There are three major factors that need to be considered—*building geometry*, *street geometry*, and *street layout*.

Building geometry describes the shape of individual buildings. For structural and economic reasons, most buildings have vertical walls arranged in rectangular or near-rectangular shapes. While not true for buildings such as cathedrals or the Guggenheim Museum, the rectilinear pattern is broadly representative of most large urban aggregations and, as such, can be exploited when scanning. However, urban buildings are often closely spaced, abutting, or employing party walls, making it difficult to distinguish individual buildings—a key feature to individual building extraction.

Street geometry describes the shape of small groups of buildings aligned along a common communication and transportation area. Typically, a street consists of two rows of parallel buildings on opposite sides of an open space. Moreover, building plots along a given street are fairly uniform in size and shape, with the result that barring topographic constraints, large parts of a city tend to have multiple streets parallel to each other. This, combined with the preferred rectilinear shape of buildings, tends to impose a strong geometric structure on the city as a whole, which can also be exploited when scanning (Fig. 3).

Street layout describes the overall geometric structure of the city. While older portions of cities can be very complex, most cities fall into three basic patterns—regular rectangular grids, radial layouts, or topographic structures. However, within radial cities, the infill between the major radial streets tends to be rectangular in nature, as does the infill between topographic boundaries. As such, a reasonable approximation of street layout is that it tends to be locally regular but may be irregular at a larger scale. This localized structure can also be exploited when scanning. For simplicity, the balance of this paper will assume that the city to be scanned can be represented locally as a rectangular grid (Fig. 3).

### *Flight Geometry*

While the flight path is notionally controllable, in practice it is easiest to fly in a straight line. Thus, most survey flight paths tend to be a set of straight lines (as opposed to a zigzag or radial pattern). Moreover, for a given altitude of flight, the LiDAR unit scans points on the ground, within a relatively fixed lateral offset (although this is dependent on the altitude of the ground). Since each straight line flown corresponds to a rectangular strip of ground scan, flight planning is principally a question of choosing the rectangular strips to be scanned in such a way that the overlap covers the desired area. Given straight-line flight paths, this means that the most straight-forward method is to fly a series of parallel flight paths, whose strips between them cover the entire

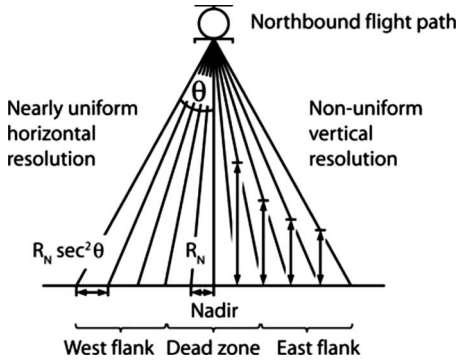


**Fig. 4.** Horizontal and vertical scan resolutions

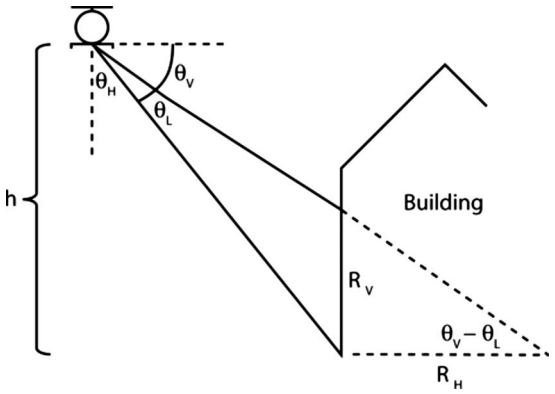


**Fig. 5.** Vertical linear resolution

area with only minimal overlap, as shown in Fig. 3. For vertical surfaces, however, further adjustments are necessary to surmount geometric impediments.

### *Vertical Scan Obliquity*

The principal geometric difficulty with LiDAR scans of vertical surfaces is that as the LiDAR scanner flies above a city, the laser beam scans a fairly narrow range of angles beneath the scanner—typically not more than 30° away from the vertical on each side. Horizontal linear resolution has previously been shown to be rather uniform in the across-track direction. This is illustrated in the left-hand side of Fig. 4, where horizontal resolution at maximum across-track offset differs from nadir ($R_N$) only by a factor of $\sec^2\theta$.

For vertical surfaces, however, as visible by the dimensions on the right side of Fig. 4, the spacing of scan points on vertical surfaces becomes increasingly larger as the vertical surfaces approach nadir. Intuitively, this is reasonable, since a vertical surface directly underneath the scanner will be parallel with the laser beam, which will, therefore, strike the entire surface. In other words, the closer a vertical surface is to nadir, the worse the vertical scan resolution on that surface will be.

Since vertical resolution is worst directly beneath the scanner, guaranteeing scan quality of a particular level requires discarding the data directly beneath the flight path, and for some distance off to the side: paradoxically, this *dead zone* of low quality vertical data are the zone of the *highest* quality horizontal scanning. The *flanks* of the scan, in contrast, generate the highest quality vertical scan and lowest quality horizontal data, as shown in Fig. 4.

From this observation, it follows that the dead zone from one flight path will have to be scanned in the flank of another flight path. Ignoring calibration issues, obtaining this flanking data are most conveniently achieved if the flank is the same width as the dead zone (or possibly a rational fraction of it). The impact on scan quality of the width of the dead zone is addressed later in the paper, but for now, consider that the dead zone and flanks are of equal width, and that each is 1/3 of the total scan width. Note that the width of the dead zone is not necessarily directly related to horizontal resolution at nadir, but rather to what is deemed to be acceptable vertical scan quality. As such, the rationale for defining the width of the dead zone varies with different types of applications and data requirements.

As in the case of linear *horizontal* resolution ($R_H$), approximations for linear *vertical* resolution ($R_V$) can be derived. Defining a vertical offset angle ($\theta_V$) related to the horizontal offset angle by $\theta_V = 90 - \theta_H$, as shown in Fig. 5, is convenient for notation. The horizontal resolution at a particular offset angle $\theta_H$ [Eq. (4)] can then be related to the *effective* vertical spacing through the expression

$$R_V = R_H \tan(\theta_V - \theta_L) \quad \text{or} \quad R_V = R_H \tan(90 - \theta_H - \theta_L) \qquad (7)$$

Just as for effective horizontal linear resolution, it would be useful to define effective vertical linear resolution for a worst case scenario. However, $R_V$ diverges to infinity at nadir, and, therefore, it is not possible to give a quantitative result for the worst case vertical linear resolution. However, the more interesting case is when a vertical surface laterally offset from nadir is being scanned. Since the vertical offset angle $\theta_V$ will be largest at ground level of the vertical surface (where $\theta_H$ is smallest), the first interval on the vertical surface is used as the worst case, with the assumption that the laser samples the vertical surface exactly at the intersection between the surface and the horizontal plane (Fig. 5).

Note that Eq. (7) is a valid approximation up to $\theta_V = \theta_H = 45°$. At this point horizontal resolution [$R_H$, Eq. (4)] starts diverging to infinity faster than $\tan(90 - \theta_H - \theta_L)$ converges to zero. However, most LiDAR hardware is only capable of $\theta_H$ up to about 30° from nadir, and the model proposed herein is valid within this range.

Fig. 6 shows how $R_H$ [Eq. (5)] and $R_V$ [Eq. (7)] vary with horizontal offset angle ($\theta_H$). The angular resolution $\theta_L$ is assumed to be 0.01° and the height used is 300 m, based on minimum allowed flyover height in urban regions. Note that an offset angle $\theta_H = 45°$ gives $R_H = R_V$.

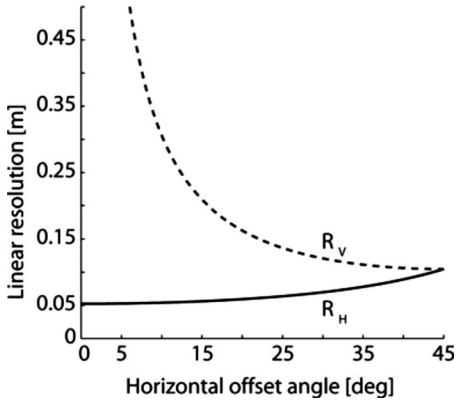


**Fig. 6.** Horizontal and vertical resolution as functions of offset angle

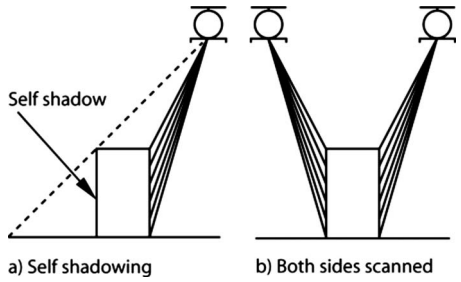


**Fig. 7.** Self shadows

### Self Shadows

In addition to dead zones caused by vertical scan obliquity, not all vertical surfaces in the scan area will appear on the scan, as a result of *shadows*—since the laser is a form of light, it is blocked by solid objects. Furthermore, as any solid object has one side facing the scanner and the other side facing away, the side facing away will be *self shadowed* by the side facing toward the scanner, as shown in Fig. 7(a). The consequence of this, shown in Fig. 7(b), is that to acquire *both* sides of a given object, there must be (as a minimum criterion) two scans: one from the left and one from the right.

Even though each flank provides good quality vertical data, it only does so for half of the vertical surfaces. Specifically, the flank to the east of the flight path will only provide data on west-facing surfaces, and the flank to the west of the flight path will only provide data on east-facing surfaces. Complete scan coverage thus requires that every building be covered from both flanks—one from each of two different flight segments (Fig. 8).

It has been established that a uniform data quality is desirable and that the highest quality vertical data are obtained in the flanking strips. Along-track resolution ($R_L$) is not subject to geometric constraints and is under the control of contractors. In the section Linear Resolution it was assumed that $R_L$ is chosen to be the same as the horizontal resolution at the nadir ($R_N$), in an attempt at achieving uniform resolution. It would, however, be more efficient to choose $R_L$ to match the vertical resolution ($R_V$) at the edges of the dead zone (i.e., the worst case). The rationale behind this is that overall resolution is never better than the worst-case scenario, and achieving better resolution in the along-track direction will not improve overall resolution; presumably, lowering the along-track resolution would lead to faster and cheaper flyover scans.

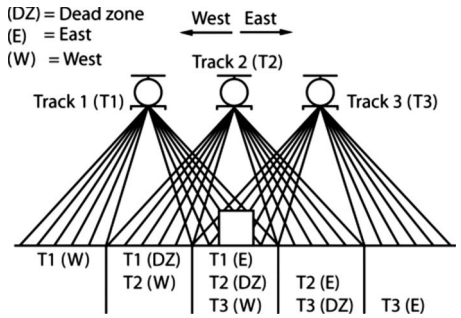


**Fig. 8.** Overlapping flanks for full coverage

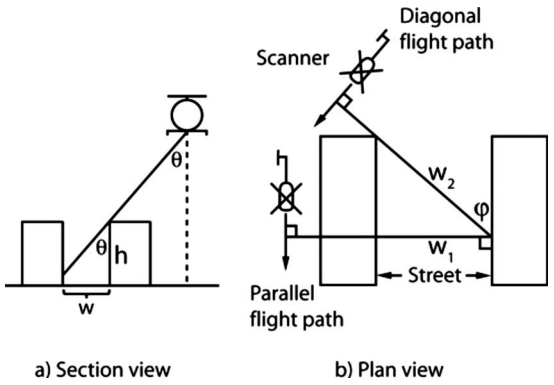


**Fig. 9.** Street shadows

### Street Shadows

While self shadows are the result of a building shadowing itself, scans may also be blocked by the effect of street shadows, in which a building is shadowed by another building on the other side of the street. Geometrically, the effect of these shadows depends on the height of the shadowing building and the distance between the two buildings, as can be seen in Fig. 9(a). If the distance, $w$, between the buildings is less than $h \tan \theta$, then the bottom of one building will be shadowed by the adjacent building. Although the building height, $h$, is immutable, the distance between buildings is measured *perpendicular* to the flight path. If the flight path is parallel to the street, these distances are minimized, as shown by width, $w_1$, in Fig. 9(b). However, flight paths at an angle to the direction of the street will effectively increase the distance between buildings, as shown by diagonal, $w_2$, in Fig. 9(b).

Using the assumed perpendicular street grid, the optimal flight angle for avoiding street shadows is 45° to the street grid. This will maximize $w_2$ for streets in both directions on, a street grid where streets run in two principal, perpendicular directions. Unfortunately, flying diagonally to the street pattern compromises the resolution on buildings in the sense that the distance between samples in the street direction [i.e., the *lateral resolution* ($R_{\mathrm{LAT}}$)] increases. Fig. 10 illustrates the relationship between linear (along-track) resolution ($R_L$) and lateral resolution $R_{\mathrm{LAT}} = R_L \sec \varphi$. This dictates that the lateral resolution suffers as the angle $\varphi$ approaches 90°. However, as long as the lateral resolution does not exceed the vertical resolution this does not matter, since the area sampling is dependent on both these distances, and will always be limited by the one that is greater. Hence, it is reasonable to sacrifice lateral resolution in exchange for minimizing street shadows.

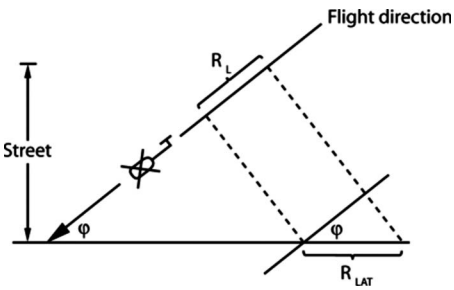


**Fig. 10.** Lateral resolution

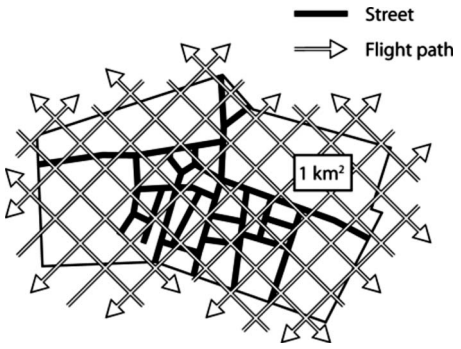


**Fig. 11.** Dublin flight plan

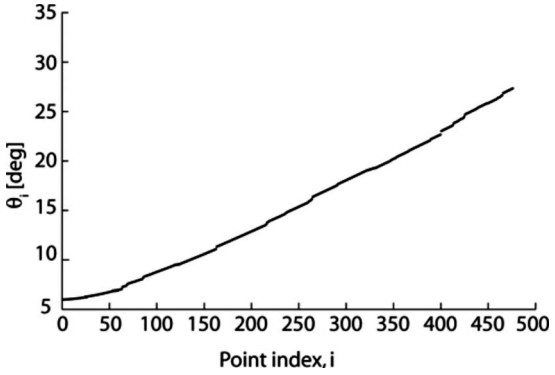


**Fig. 12.** Horizontal offset angle

## Flight Planning

As noted above, the simplest approach is to set the dead zone equal in width to the flanks; for example, for a total scan width of 300 m, the dead zone and flanks should each be 100 m wide. From Fig. 8, setting the distance between the flight paths equal to this width is shown, although a slight reduction may be desirable to achieve some additional overlap and avoid lacunae in the data. As such, the ideal flight path will consist of a series of parallel lines diagonal to the local street grid, spaced at a distance of 1/3 the total scan width (or possibly a rational fraction of it) from each other, in order to guarantee that each building is correctly scanned on all principal faces with a maximum of scan resolution and a minimum of shadowing. The specific amount of overlap chosen should reflect the along-track resolution and the importance of high data quality on vertical surfaces, and as such, is somewhat project specific.

Street patterns are never perfect grids in practice, and, therefore, trade-offs have to be made. One strategy would be to fly diagonally to as many streets as possible, regardless of individual street widths. This makes sense because the effective gain in street width by flying diagonally is the same, regardless of street width. A slightly more sophisticated approach would be to assign importance weights to the streets, and use these weights as decision factors for optimizing the flight path. One could also imagine using a numerical optimization method that takes a street pattern as input and computes a flight plan that flies at as close to 45° as possible to as many streets as possible. Finally, if a 3D model of the study area exists already, this may be used as input and would give an even better flight plan since building geometries and shadowing effects could be taken into account. However, no algorithms for this type of flight planning exist at present, and in the case study presented next, the flight plan was manually designed to roughly meet the 45° angle criterion.

## Case Study: Dublin City Center

Up to this point the discussions in this paper have been of a strictly theoretical nature. The validity of these results was confirmed by developing an aerial LiDAR flight plan to scan parts of Dublin city center in order to acquire facades for further processing. Fig. 11 shows the flight path overlaid on the major street grid. Since Dublin does not have a perfectly regular grid, the strictly ideal case of diagonal flight paths was not possible. However, like many other urban centers, there is a tendency toward east-west, north-south street orientation, and the dominant directions of the flight segments were chosen to be northeast and southwest.

Three principal hypotheses were tested in this case study: (1) linear resolution can be predicted from scanner parameters on horizontal and vertical surfaces; (2) generous amounts of flight strip overlap vastly improves data quality on vertical surfaces by eliminating dependence on data from dead zones; and (3) adherence to the flight planning discussed in this article leads to scans with sufficient vertical resolution that façade elements are clearly visible.

### *Linear Resolution*

To confirm the predictions of linear resolution, point samples from a representative sweep or *scan line* perpendicular to the flight direction were extracted. Each scan line has approximately 1,000 such points. Since the data, as delivered, were not segregated by scan line, it was necessary to do so manually. Since point samples from a single scan line have identical time stamps, all point samples from a particular scan line can be grouped by clustering point samples with identical time stamps. For simplicity of the example provided below, only points on one side of the nadir were chosen. Thus, the horizontal offset angles $\theta_H$ for the point samples are strictly increasing, which makes the plots easier to read.

For each extracted point sample, the interpolated position of the scanner, $P_s=(x_s, y_s, z_s)$, and point position, $P_i=(x_i, y_i, z_i)$, were retrieved from the data. Scanner position over time is given in the same frame of reference as the time stamps for the point samples. However, scanner position is given at time intervals that are larger than the difference in time between consecutive scan lines. Therefore, it is unlikely that scanner position data exists for the exact time stamp of the point samples of a scan line. For this reason, scanner position, $P_s$, is component-wise linearly interpolated from the two nearest given scanner positions in time. Further, the horizontal offset angles $\theta_i$ were computed using the following formula

$$\Delta x = |x_s - x_i|$$

$$\Delta y = |y_s - y_i|$$

$$\Delta z = |z_s - z_i|$$

$$\theta_i = \tan^{-1}(\sqrt{\Delta x^2 + \Delta y^2}/\Delta z) \tag{8}$$

Extracted points were sorted with respect to increasing $\theta_i$, i.e., such that $\theta_{i+1} > \theta_i$. This ordered them in a fashion that corresponds to being consecutive samples in a single scan line. Fig. 12 plots the sorted $\theta_i$ in order, from lowest to highest; since the

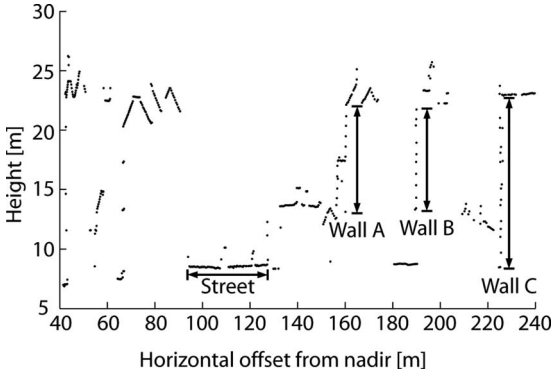


**Fig. 13.** Scan line height profile

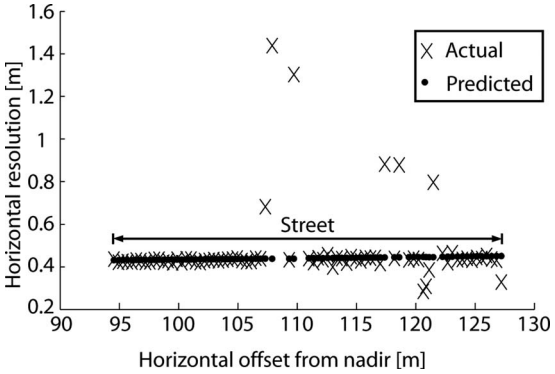


**Fig. 14.** Horizontal resolution prediction

scanner takes periodic samples (i.e., $\theta_{i+1} \approx \theta_i + \theta_L$), it was predicted that this plot should be linear. As shown in the figure, there is close but not perfect agreement with this, indicating that the sorting procedure established the correct (or nearly correct) ordering of the samples. Any deviation from this is assumed to be due to noisy range measurements, scanner position interpolation, and the lack of compensation for scanner pitch and roll.

Since the scan line is essentially linear, it can be plotted. By computing the horizontal distance $d_i$ to nadir [i.e. $(x_s, y_s, 0)$]

$$\Delta x = |x_i - x_s|$$

$$\Delta y = |y_i - y_s|$$

$$d_i = \sqrt{\Delta x^2 + \Delta y^2} \tag{9}$$

and plotting $(d_i, z_i)$ cross-sectional view (height profile), can be generated as shown in Fig. 13. Note that the smallest horizontal offset distance in the plot is 40 m. When extracting points, it was desirable to avoid working with points close to nadir in order to avoid infinite vertical resolution prediction further on, as discussed below. However, those issues do not exist as the horizontal distances increase, and the extracted points, therefore, extend to the maximum horizontal offset. This plot clearly shows the high horizontal resolution on the street combined with the lower vertical resolution on walls.

Recall from Eqs. (5) and (7) that expected formulas for horizontal and vertical linear resolution were calculated. Eq. (5) assumed that two consecutive point samples had the same vertical ($z$) coordinate. For points on the ground such as those marked as *Street* in Fig. 13, this is a reasonable approximation. For points on walls, diagonal elements such as roofs, or on trees, cars or other features, greater variance is expected, but there are enough points along ground surfaces to make a comparative plot meaningful. For a single scan line, the predicted horizontal resolution comes directly from Eq. (5), while the measured horizontal resolution is taken to be the horizontal distance to the next consecutive point. Fig. 14 shows the result of this plot for the points marked as *Street* in Fig. 13. Based on scanner functionality, if a surface was completely horizontal the distribution of points follows Eq. (6). The data in Fig. 14, with the exception of some outliers, which can be attributed to shadowing effects from a vehicle such as a bus, show that the agreement for the prediction with horizontal surfaces is extremely good.

Similarly, Fig. 15 compares the actual vertical resolution against that predicted by Eq. (7). Here, actual vertical resolution was computed as the vertical distance to the next consecutive point. Fig. 15 shows the plotted vertical resolution for the sequence of apparent wall/roof elements at the right-hand end of the height profile shown in Fig. 13. This plot is harder to interpret, as wall elements share essentially the same horizontal offset. However, horizontal surfaces are flat and, thus, the points representing them have nearly zero difference in the vertical direction. More importantly, for the vertical surfaces (i.e., the building walls) the actual resolutions cluster close to the predicted values, especially near 160, 190, and 225 m from nadir (marked with circles in Fig. 15), which agrees with the presence of walls noted in the scan line height profile (Fig. 13). An important observation is that even for a set of points all with nearly identical horizontal offsets it is unlikely that the distances between these will match perfectly the predicted resolution. Most likely the highest point in such a set is actually sampled on an adjoining nonvertical surface (i.e., roof); thereby appearing to belong to the wall, when in fact this is not the case. Similarly, it is unlikely for the lowest point sample on a wall to be at the intersection of the wall and the horizontal plane. This may lead to situations where vertical distance is computed between a point on a horizontal surface and a point only a short distance up the wall, resulting in a small measured vertical resolution where a large one is predicted. In practice, this means that some outliers are to be expected, even when samples appear to be from the same vertical surface.

Moreover, in this study the vertical distance between consecutive points is described as an absolute value. Negative vertical distances would arise when consecutive points are sampled on separate surfaces with different elevations. This occurs frequently because of building shadowing, where the building wall not facing the scanner is not sampled. These situations arise where the first of two consecutive points is sampled on the building roof, and the next one is sampled on a different building or street.

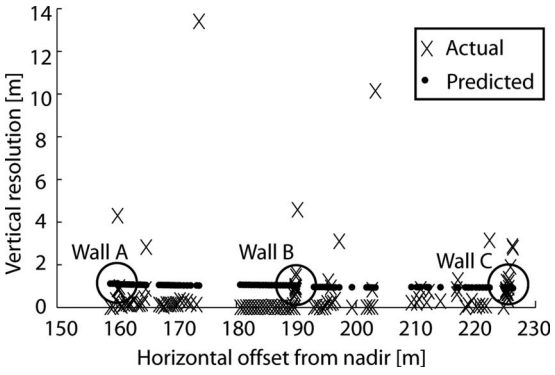


**Fig. 15.** Vertical resolution prediction

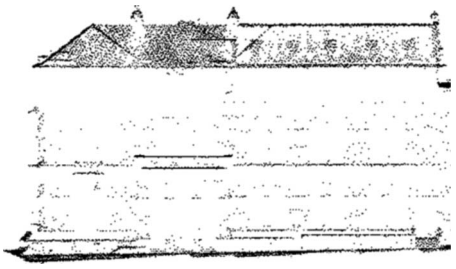

**Fig. 16.** Single overlap

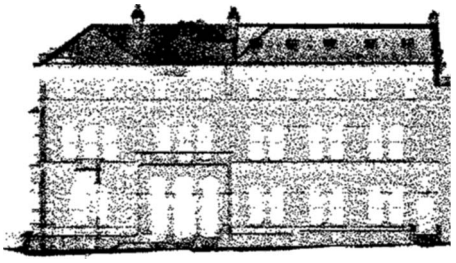

**Fig. 17.** Multiple overlap

The results of the enhanced flight plan are most clearly compared against the scanner output from a single pass (akin to traditional nonoverlapping flight path data acquisition) for one isolated façade. Fig. 16 shows the samples on the facade acquired during a single flight strip. Although the overall configuration of the facade is visible, structural details are not. In comparison, Fig. 17, with the multiple overlap, clearly shows the individual window and door openings in the façade, although shadowing effects from the eaves still occur at the top of the wall. This data set is now available at http://lidar.ucd.ie/index.html.

## Conclusions

Current aerial LiDAR equipment has the potential to return significant amounts of data related to the vertical details of buildings in urban environments. The successful acquisition of such data are, however, highly dependent on understanding where high quality data are acquired with respect to the flight plan, namely in the flanks, instead of at nadir. Therefore, the flight plan should be designed so strip overlap accounts for dead zones directly beneath the scanner. Further, flying diagonally to the main orientation of the structures of interest reduces the issue of blind spots in the data caused by shadowing. Although both of these aspects are readily achievable within the current state of practice, both are counterintuitive. Traditional practice has to date focused on the capture of surfaces in the horizontal plane, as opposed to those in the vertical. The principles presented here allow for more versatile data sets due to the fact that a higher level of detail is present. The presented method works toward uniform resolution by sacrificing lateral resolution in exchange for higher vertical resolution and fewer blind spots in the data, which are major impediments for resolution uniformity. Focusing on vertical façades makes sense in urban visualizations since façades have more diverse appearances than for instance roofs or streets. This information is increasingly needed for digital models of cities. The algorithm presented herein achieves vastly improved output while incurring only minimal extra cost since it is simply a different way of thinking about sampling and is therefore, simple to incorporate into existing flyover programs.

## Acknowledgments

Support for this work was generously provided by Science Foundation Ireland, Grant No. 05/PICA/I830, GUILD: Generating Urban Infrastructures from LiDAR Data.

## Notation

*The following symbols are used in this paper:*

$A_L$ = laser footprint area (m);
$d_i$ = horizontal distance to nadir for point $i$ of a single scan line (m);
$h$ = height (m);
$P_i$ = position of point $i$ of a single scan line (m);
$P_s$ = scanner position (m);
$R_H$ = horizontal resolution in across-track direction (m);
$R_L$ = along-track resolution (m);
$R_{\mathrm{LAT}}$ = lateral resolution (m);
$R_S$ = surface resolution ($m^2$/scan point);
$R_N$ = horizontal resolution at nadir (m);
$R_W$ = effective horizontal linear resolution (m);
$S$ = scan point density (scan points/$m^2$);
$\gamma$ = beam divergence (radians);
$\theta_H$ = horizontal offset angle (degrees);
$\theta_i$ = horizontal offset angle for point $i$ of a single scan line (degrees);
$\theta_L$ = angular resolution (degrees);
$\theta_V$ = vertical offset angle (degrees); and
$\theta_W$ = maximum horizontal offset angle (degrees).

## References

Andersen, H.-E., McGaughey, R. J., and Reutebuch, S. E. (2005). "Estimating forest canopy fuel parameters using LIDAR data." *Remote Sens. Environ.*, 94, 441–449.

Axelsson, P. (1999). "Processing of laser scanner data—Algorithms and applications." *ISPRS J. Photogramm. Remote Sens.*, 54(2–3), 138–147.

Baltsavias, E. P. (1999a). "Airborne laser scanning: Existing systems and firms and other resources." *ISPRS J. Photogramm. Remote Sens.*, 54(2–3), 164–198.

Baltsavias, E. P. (1999b). "Airborne laser scanning: Basic relations and formulas." *ISPRS J. Photogramm. Remote Sens.*, 54(2–3), 199–214.

Dorninger, P., and Nothegger, C. (2007). "3D segmentation of unstructured point clouds for building modeling." *Int. Arch. Photogramm. Remote Sens. Spat. Inf. Sci.*, 36, 191–196.

Filin, S., Akel, N. A., and Doytsher, Y. (2007) "Detection and reconstruction of free form surfaces from airborne laser scanning data." *Int. Arch. Photogramm. Remote Sens. Spat. Inf. Sci.*, 36, 119–124.

Forlani, G., Nardinocchi, C., Scaioni, M., and Zingaretti, P. (2006). "Complete classification of raw LIDAR data and 3D reconstruction of buildings." *Pattern Anal. Appl.*, 8, 357–374.

Früh, C., and Zakhor, A. (2003). "Constructing 3D city models by merging aerial and ground views." *IEEE Comput. Graphics Appl.*, 23(6), 52–61.

Haala, N., and Brenner, C. (1999). "Extraction of buildings and trees in urban environments." *ISPRS J. Photogramm. Remote Sens.*, 54(2–3), 130–137.

Hamill, J., and O'Sullivan, C. (2003). "Virtual Dublin—A framework for real-time urban simulation." *J. Winter School of Computer Graphics*, 11(1), 221–225.

Hollaus, M., Wagner, W., and Kraus, K. (2005). "Airborne laser scanning and usefulness for hydrological models." *Adv. Geosci.*, 5, 57–63.

Kazhdan, M., Bolitho, M., and Hoppe, H. (2006). "Poission surface reconstruction." *Proc., 4th Eurographics Symposium on Geometry Processing*, Eurographics Association, Aire-la-Ville, Switzerland, 61–70.

Kevany, M. J. (2003). "GIS in the World Trade Center attack—Trial by fire." *Comput. Environ. Urban Syst.*, 27(6), 571–583.

Laefer, D., Fitzgerald, M., Maloney, E., Coyne, D., Lennon, D., and Morrish, S. W. (2009). "LiDAR lateral image degradation and its implications for condition assessment and structural health monitoring." *Struct. Eng. Int. (IABSE, Zurich, Switzerland)*, 19(2), 184–189.

Laefer, D., and Pradhan, A. (2006). "Evacuation route selection based on tree-based hazards using LiDAR and GIS." *J. Transp. Eng.*, 132(4), 312–320.

Latypov, D. (2002). "Estimating relative lidar accuracy information from overlapping flight lines." *ISPRS J. Photogramm. Remote Sens.*, 56, 236–245.

Liu, B., Yi, F., and Yu, C. M. (2005). "Methods for optical adjustment in lidar systems." *Appl. Opt.*, 44, 1480–1484.

Maas, H.-G., and Vosselman, G. (1999). "Two algorithms for extracting building models from raw laser altimetry data." *ISPRS J. Photogramm. Remote Sens.*, 54(2–3), 153–163.

Rottensteiner, F. (2003). "Automatic generation of high-quality building models from Lidar data." *IEEE Comput. Graphics Appl.*, 23(6), 42–50.

Vosselman, G., Gorte, B. G. H., Sithole, G., and Rabbani, T. (2004) "Recognising structure in laser scanner point clouds." *Int. Arch. Photogramm. Remote Sens. Spat. Inf. Sci.*, 46(8/W2), 33–38.

Wehr, A., and Lohr, U. (1999). "Airborne laser scanning—An introduction and overview." *ISPRS J. Photogramm. Remote Sens.*, 54(2–3), 68–82.